Catalysis Science & Technology

ROYAL SOCIETY OF CHEMISTRY

PAPER

View Article Online
View Journal | View Issue

Cite this: *Catal. Sci. Technol.*, 2025, **15**, 7504

Strategic integration of pendant –COOH and –NH sites in a Zn-MOF for hydrogen-bond donating organocatalysis in the Friedel–Crafts alkylation reaction of indoles with β-nitrostyrenes

Vandana Sharma and Sanjay K. Mandal *

Hydrogen-bond donating (HBD) sites in catalysts play a pivotal role in facilitating precise substrate activation and transition state stabilization, thereby enhancing both reactivity and selectivity in a wide range of C–C bond forming transformations. The orientation of these HBD sites in the vicinity, for the synergistic activity of catalysts, is also challenging to achieve, particularly in heterogeneous catalysis. In this work, we designed and synthesized a new eminently robust 3D metal–organic framework (MOF), $[Zn_4(H(D\text{-}GluBenz))_4(H_2O)_2]_n$ [**Zn-(D-GluBenz)**], where the D-glutamic acid-based H_3(D-GluBenz) ligand acts as a dicarboxylate for a perfect strategic integration of both –COOH and –NH pendant sites for the first time. This architectural precision provides a unique active environment that makes it a hydrogen-bond donating organocatalyst for the efficient Friedel–Crafts alkylation of indoles with β-nitrostyrenes under significantly milder conditions than previously reported. In addition to having a broad substrate scope, **Zn-(D-GluBenz)** demonstrates excellent recyclability and robust heterogeneity. The key hydrogen bonding interactions between the HBD sites of **Zn-(D-GluBenz)** and the nitro group of β-nitrostyrene are confirmed through fluorescence spectroscopy, underscoring its organocatalytic nature. This work highlights the untapped potential of amino acid-based MOFs as versatile platforms for sustainable HBD-driven organocatalysis.

Received 7th August 2025,
Accepted 16th October 2025

DOI: 10.1039/d5cy00966a

rsc.li/catalysis

Introduction

Hydrogen-bond donating (HBD) catalysis has become a cornerstone of modern organocatalysis, offering an elegant, non-covalent approach to substrate activation. It plays a pivotal role in enabling a broad range of organic transformations, particularly those requiring activation of electrophilic substrates such as nitroalkenes, imines, and carbonyl compounds. By forming directional hydrogen bonds with these electrophilic substrates, HBD catalysts can significantly lower activation barriers and enforce stereochemical control in these transformations.[1–3] Mimicking the precise control observed in enzymatic systems, HBD catalysts stabilize transition states and enhance stereocontrol without the need for metal centers.[4] Despite its conceptual simplicity and broad utility, early HBD catalysts faced notable limitations. In particular, homogeneous organocatalysts, such as thioureas, squaramides, and ureas, which are highly effective, often suffer from poor recyclability, limited stability under reaction conditions, product inhibition, and self-quenching due to intramolecular hydrogen bonding or substrate competitions.[5,6]

Therefore, recent advances have moved toward heterogeneous HBD catalysis, where immobilization of the hydrogen-bond sites onto the solid supports overcomes many drawbacks of the homogeneous systems. Among these, metal–organic frameworks (MOFs) have emerged as highly promising platforms. MOFs offer a unique combination of well-defined porosity, high surface area, and structural tunability, allowing precise spatial organization of HBD sites.[7,8] This architecture not only stabilizes the HBD sites but also enables the spatial control over their orientation, enhanced stability under reaction conditions, and facile recovery and reuse, addressing key drawbacks of the traditional homogeneous systems.[9,10] This integration of traditional organocatalysis principles into porous crystalline materials represents a significant leap forward in the development of sustainable and efficient catalytic systems. In recent years, MOFs functionalized with thiourea, squaramide and urea moieties in the carboxylate linkers have been widely used in key transformations, such as the Meerwein Ponndorf Verley reduction, Hantzch condensation reaction, Friedel–Crafts alkylation reaction of indoles with β-nitrostyrenes, cyanosilylation reaction, Henry reaction, Morita–Baylis

Department of Chemical Sciences, Indian Institute of Science Education and Research Mohali, Sector 81, Manauli PO, S.A.S. Nagar, Mohali, Punjab 140306, India. E-mail: sanjaymandal@iisermohali.ac.in

Hillman reaction, methanolysis of epoxides and CO_2 fixation in epoxides.[11–14]

Out of all these transformations, the Friedel–Crafts alkylation reaction remains a cornerstone in organic synthesis, facilitating the formation of carbon–carbon bonds between aromatic compounds and electrophiles, playing a crucial role in the synthesis of fine chemicals, pharmaceuticals, and natural products.[15] Indoles represent a crucial structural motif found in a wide array of natural products, pharmaceuticals, and biologically active compounds, making their functionalization a topic of great synthetic interest.[16–18] Among various transformations, the C3-alkylation of indoles is particularly significant due to its role in constructing complex molecular architectures.[19–21] In this context, β-nitrostyrene has emerged as a highly efficient and versatile electrophile, which provides access to nitroalkylated indole derivatives that can be further converted into valuable amine-containing scaffolds. The broad reactivity and synthetic utility of β-nitrostyrene continue to drive its application in indole-based catalytic transformations.[22–24] In the case of β-nitrostyrene, the nitro group serves as a strong hydrogen bond acceptor and HBD-functionalized MOFs can effectively polarize the electron-deficient alkene, facilitating nucleophilic attack by indole at the C3 position. However, catalysts based on HBD-functionalized MOFs often face limitations such as the need for high catalyst loadings, prolonged reaction times, and complex, multistep syntheses typically involving post-synthetic modification (PSM) or post-synthetic exchange (PSE) strategies.[25–32]

Examples of MOF-based catalysts utilized for the Friedel–Crafts alkylation reaction of indoles with β-nitrostyrenes, featuring HBD groups such as ureas and squaramides, were the first series to mimic homogeneous organocatalysts (overcoming the self-quenching issue). In these catalysts, two N–H bonds separated by one or two carbon atoms were involved in the hydrogen bonding with the nitro group of β-nitrostyrenes (Scheme 1a and b).[33,34] The third type was reported by our group, where the free NH_2 group of a metal-coordinated primary amide group provided both N–H bonds for interacting with the nitro group of β-nitrostyrenes (Scheme 1c).[35] More recently, two O–H bonds from two free carboxylic acids (Scheme 1d)[36] or two N–H bonds of an amine group attached to an aromatic ring (Scheme 1e)[28] have been well-documented in the literature, highlighting their effectiveness in HBD-driven catalysis. In view of these diverse systems, we envisioned making an advancement with the incorporation of amino acid-based tricarboxylic acids into MOFs. These amino acid-derived catalysts stand out for their natural abundance and dual hydrogen bond donating functionalities, namely, the –OH moiety of a free carboxylic acid group and the –NH moiety separated by two carbon atoms.[5,37] However, the challenge was to have a free COOH group along with the N–H moiety.

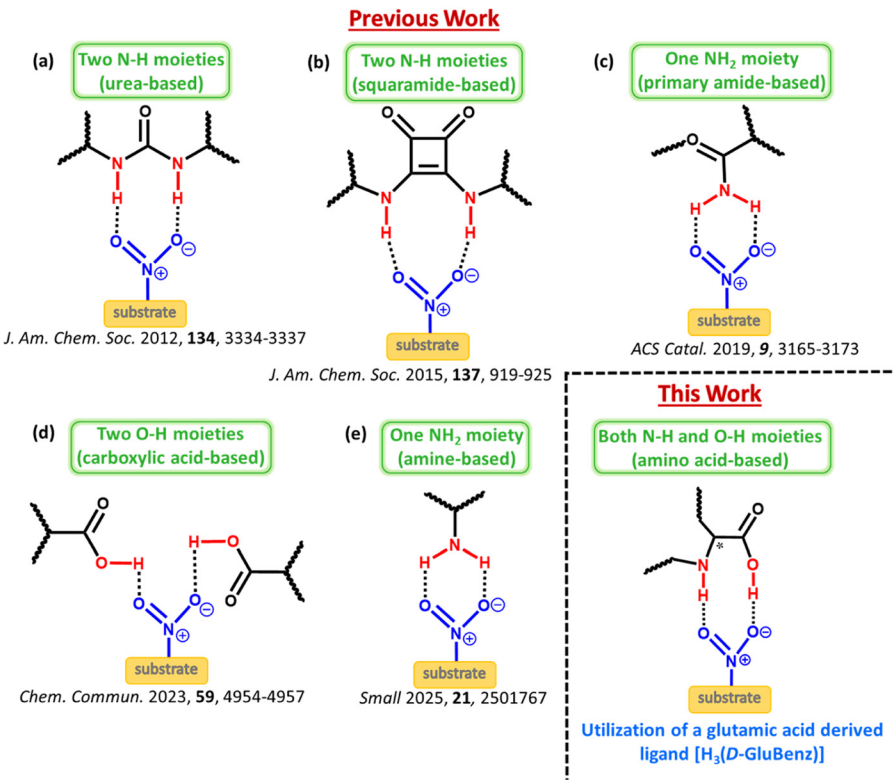

Scheme 1 Background and importance of this work: hydrogen bond-assisted activation of nitro-functionalized substrates by urea, squaramide, primary amide, carboxylic acid, amine and glutamic acid-derived ligand-based MOFs.

Building upon these advancements, this work reports the development of a novel Zn-based metal–organic framework $[Zn_4(H(D\text{-GluBenz}))_4(H_2O)_2]_n$ **[Zn-(D-GluBenz)]** using a new glutamic acid-derived ligand, (*R*)-2-((4-carboxybenzyl)amino) pentanedioic acid, H_3(D-GluBenz) (for its structure, see Scheme 2) for the availability of two intrinsic HBD sites, such as –COOH and –NH moieties. With this strategy, we aimed to demonstrate its efficacy as a heterogeneous catalyst in promoting the reaction under mild, environmentally benign conditions while also highlighting its recyclability and potential for broader applications in sustainable organic synthesis. As an example, it is utilized in the Friedel–Crafts alkylation reaction of indoles with β-nitrostyrenes under significantly milder conditions than previously reported. In addition to having a broad substrate scope, the catalyst demonstrates excellent recyclability and robust heterogeneity. A strong experimental support for the proposed catalytic mechanism is provided by the fluorescence studies, which reveals a significant reduction in the emission intensity of **Zn-(D-GluBenz)** upon incremental addition of β-nitrostyrene. This pronounced quenching effect highlights the hydrogen bonding interaction between both –COOH and –NH groups of the catalyst and the nitro group of β-nitrostyrene, thereby affirming the crucial role of these interactions in substrate activation. To the best of our knowledge, there is no report in the literature for a catalyst with both –NH and –COOH moieties functioning as HBD sites. This study not only advances a sustainable protocol for indole functionalization but also highlights the untapped potential of MOFs as H-bond-driven organocatalytic platforms offering a new direction in developing environmentally benign and highly tunable catalytic systems.

Experimental section

The Materials and characterization methods section is described in the SI.

Synthesis of H_3(D-GluBenz)

In a 25 mL round-bottom flask (RBF), a clear solution of D-glutamic acid (118 mg, 0.8 mmol) and NaOH (96 mg, 2.4 mmol) in 7 mL of MeOH and H_2O (3 : 1, v/v) was prepared. After stirring the solution for 20 min, terephthalaldehydic acid (120 mg, 0.8 mmol) was added slowly to it with stirring. The imine formation resulted in a white precipitate after stirring for 80 min. Next, the *in situ* reduction was done at 0 °C using an ice bath by adding sodium borohydride (30 mg, 0.8 mmol) to the solution and stirring for another 6 h at 25 °C. The reduced crude product was then extracted by solvent removal under a vacuum. Further, this obtained white crude solid was dissolved in 2.5 mL of water and acidified with a slow addition of 3.2 mL of a 2 N HCl solution. The white-colored pure product was filtered, washed thoroughly with water (3 × 2 mL), then with methanol (3 × 1 mL) and air-dried. Yield: 183 mg (82%). M.p. 190 °C. HRMS (ESI) *m*/*z*: calcd. 348.0413 ($[M + H + 3Na]^+$):, ^{1}H NMR (400 MHz, D_2O): δ 7.67 (d, 2H), 7.26 (d, 2H), 3.5 (dd, 2H), 2.98 (t, 1H), 2.01 (m, 2H), 1.64 (m, 2H) ppm. ^{13}C NMR (100 MHz, D_2O): δ 29.6, 34.1, 50.8, 63.0, 128.3, 128.9, 134.9, 141.9, 175.5, 181.2, 182.5 ppm. FTIR (KBr) ν_{max}/cm^{-1}: 3429 (br), 3006 (br), 1698 (s), 1653 (s), 1601 (s), 1395 (m), 1307 (m), 756 (m).

Synthesis of $[Zn_4(H(D\text{-GluBenz}))_4(H_2O)_2]_n$ [Zn-(D-GluBenz)]

For the one-pot assembly in a 5 mL Teflon reactor, a mixture of H_3(D-GluBenz) (22.6 mg, 0.08 mmol) and $Zn(OAc)_2{\cdot}2H_2O$ (17.6 mg, 0.08 mmol) in 1.5 mL of EtOH and H_2O (1 : 1, v/v) was taken. After sealing the reactor inside the autoclave jacket tightly, it was kept in a programmable oven. The reactor was heated for 48 h at 60 °C, then cooled slowly at 1 °C h^{-1} to 25 °C. The white solid was filtered, rinsed with water (5 × 1 mL) and ethanol (4 × 1 mL), then air-dried. Yield: 21 mg (75%), based on the ligand. Elemental analysis calculated for $C_{52}H_{56}N_4O_{26}Zn_4$ (MW 1414.54 g mol^{-1}): C, 44.15; H, 3.99; N, 3.96% and found: C, 44.19; H, 3.915; N, 3.98%. Selected FTIR (KBr) ν_{max}/cm^{-1}: 3428 (br), 2999 (m), 2779 (m), 1652 (s), 1607 (s), 1550 (s), 1424 (s), 1391 (s), 763 (s).

General procedure for the Friedel–Crafts alkylation reaction

For the standard catalytic reaction, in a 5 mL RBF, the indole (18 mg, 0.15 mmol), β-nitrostyrene (15 mg, 0.1 mmol), and 1 mL of solvent were stirred along with the required amount of catalyst at the preferred temperature for a suitable time. Afterward, the solid catalyst was separated by centrifugation, and the solvent from the supernatant was dried under reduced pressure. The resulting crude product was dissolved in $CDCl_3$ for conversion (%) analysis using ^{1}H NMR spectroscopy. The product was purified using column chromatography with petroleum ether and ethyl acetate (10 : 1, v/v) eluent and was analyzed by ^{1}H and ^{13}C NMR spectroscopy.

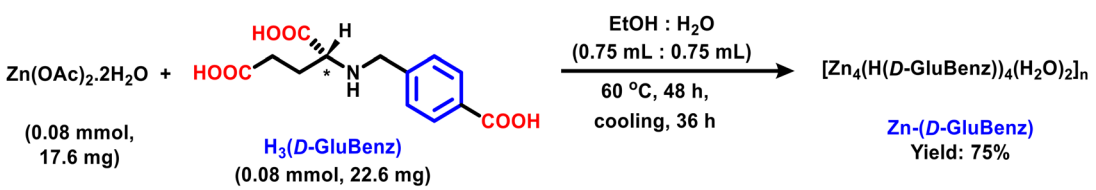

Scheme 2 Synthesis of Zn-(D-GluBenz).

Recycling of the catalyst

The catalyst recuperated from centrifugation was washed with chloroform (2 × 1 mL) and air dried until completely dry. The catalyst was then reactivated in a vacuum oven at 120 °C for 5 h and used in the next catalytic cycle. This recyclability test was carried out four times, and the FESEM and PXRD analysis confirmed the structural integrity of the catalyst.

Results and discussion

Synthesis and characterization

The synthesis of the H_3(D-GluBenz) ligand was achieved using a typical Schiff-base reaction, yielding 82% pure ligand (Scheme S1). The reaction process includes the formation of an imine intermediate and subsequent *in situ* reduction by sodium borohydride. The pure white product was precipitated out by acidification up to pH ~1. The optimized reaction conditions were then utilized to obtain it on a multigram scale. The characterization of H_3(D-GluBenz) was done by standard analytical techniques, *i.e.*, $^1H/^{13}C$ NMR and FTIR spectroscopy, HRMS and circular dichroism (CD) spectroscopy. The FTIR analysis of H_3(D-GluBenz) confirms the three distinct carboxylic acids (marked as 'a', 'b', and 'c' in Fig. S1) with respective peaks noted at 1698, 1653, and 1601 cm^{-1}, respectively (Fig. 1a). The peak at 3006 cm^{-1} is also noted for the secondary amine group. Similarly, the peak at 3429 cm^{-1} is due to the OH group. The analysis of ^1H and ^{13}C NMR spectra of Na_3(D-GluBenz) shows peaks at specific δ values for their respective protons and carbons without any extra peaks, which also validates its purity (Fig. S2 and S3). The HRMS data of Na_3(D-GluBenz) shows an m/z value of 348.0413, corroborating its molar mass, thus verifying the successful synthesis of the H_3(D-GluBenz) ligand (Fig. S4). A comparison of the CD spectrum of Na_3(D-GluBenz) with that of previously reported Na_3(L-GluBenz)[38] showed exactly opposite Cotton effects, with a positive signal at 237 nm and a negative one at 218 nm (Fig. S5).

Zn-(D-GluBenz) was synthesized by a one-pot assembly of $Zn(OAc)_2{\cdot}2H_2O$ and H_3(D-GluBenz) in an EtOH and H_2O (1 : 1, v/v) solvent system under moderate temperature with 75% yield (Scheme 2). Its gram-scale synthesis under the same conditions did not affect the % yield. Further, various characterization techniques were utilized to characterize **Zn-(D-GluBenz)**. A comparison of the FTIR spectra of the **Zn-(D-GluBenz)** and H_3(D-GluBenz) ligands (Fig. 1a) showed that the specific peak at 1652 cm^{-1} for the carboxylic acid 'b' of the ligand is retained.

This withholding of the peak confirms the uncoordinated form of 'b' carboxylic acid (Fig. S1). For the other coordinated carboxylates 'a' and 'c' to the Zn(II) centers, the distinct peaks for asymmetric vibration are at 1607 and 1550 cm^{-1}, and symmetric vibrations are at 1424 and 1391 cm^{-1}, respectively (Fig. 1a). The difference between asymmetric and symmetric vibrations is 183 and 159 cm^{-1} for 'a' and 'c' carboxylates, respectively. Two other broad peaks at 3428 and

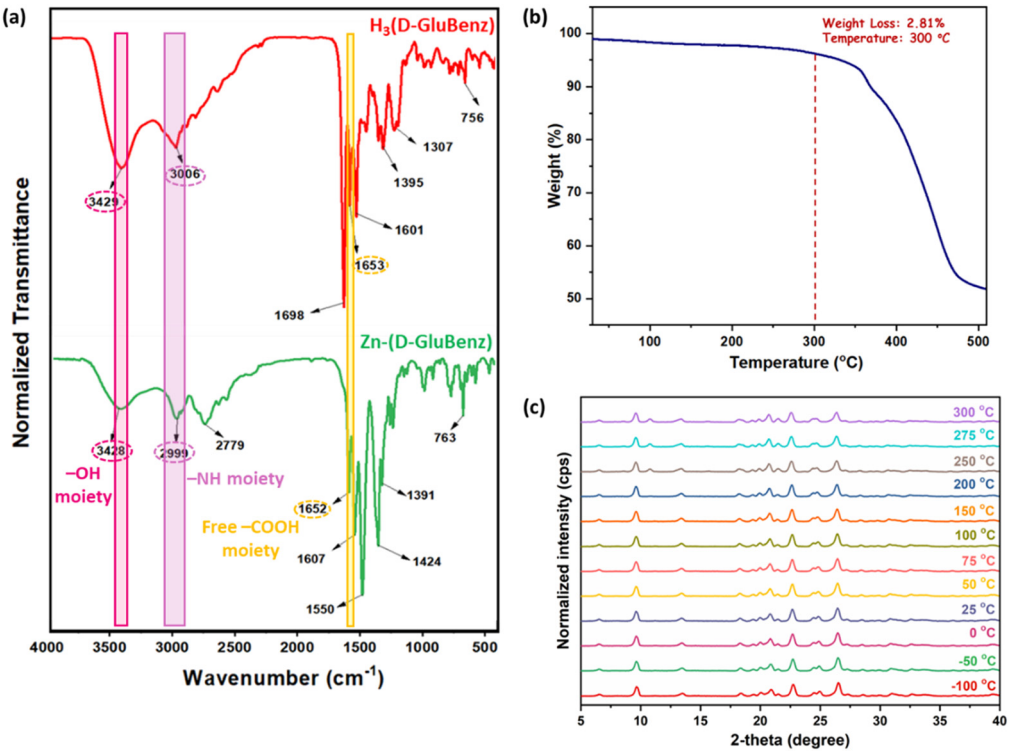

Fig. 1 (a) Comparison of FTIR spectra of H_3(D-GluBenz) and **Zn-(D-GluBenz)**, highlighting the catalytic sites, (b) thermogravimetric analysis profile and (c) VT PXRD patterns from −100 to +300 °C of **Zn-(D-GluBenz)**.

2999 cm^{-1} validate the vibrational peaks of the coordinated water molecule and the secondary amine group, respectively. Furthermore, its CHN microanalysis confirms the proposed formula with a $Zn_4(–COO)_6$ core, where four Zn(II) centers are bridged by six carboxylate groups as supported by FTIR data.[38,39] Utilizing all these information, the geometry-optimized structure of **Zn-(D-GluBenz)** obtained by *BIOVIA Materials Studio 21.1* program using the DMol^3 module with a GGA/BLYP basis set is shown in Fig. S6.[40] For the coordination of type a and c carboxylates of the ligand (leaving type b as a free carboxylic acid group), six out of eight carboxylate groups from the four ligands are in a bidentate bridging mode with four Zn(II) centers in the core, whereas the other two carboxylate groups are in a monodentate binding mode to two Zn(II) centers. Thus, two Zn(II) centers are coordinated with four bridging carboxylate O atoms and the other two are coordinated with two bridging carboxylate oxygen atoms, one monodentate carboxylate atom and one water molecule, resulting in all tetracoordinated Zn(II) centers.

Thermogravimetric analysis (TGA) of **Zn-(D-GluBenz)** reveals its robustness up to 300 °C under a nitrogen environment. The observed weight loss between 30 and 300 °C of only 2.81 wt% matches well with the calculated weight loss for two coordinated water molecules of 2.53 wt% (Fig. 1b). On the other hand, the large weight loss 38.7 wt% (calcd 39.4 wt%) between 300 and 485 °C indicates the loss of a single unit of the H_3(D-GluBenz) ligand. *In situ* variable-temperature (VT) PXRD from −100 to +300 °C was also conducted to check for its crystallinity and thermal stability. As shown in Fig. 1c, there is no change in the pattern and intensity of peaks over the complete temperature range, confirming its thermal stability, structural robustness, and crystallinity. The CD spectrum of **Zn-(D-GluBenz)** also confirms its chiral nature by showing the negative Cotton effect (Fig. S7).

The morphological analysis done by FESEM and TEM (Fig. 2a and b) reveals the agglomeration of flake-like particles. On the scanning of one of the flakes using high-resolution (HR) TEM (Fig. 2c), the obtained diffraction planes and lattice fringes (Fig. 2e) were utilized for the average *d*-spacing value calculation (0.258 nm) as shown in Fig. 2f. Furthermore, the application of an inverse fast Fourier transform (FFT) calculation for the selected area electron diffraction (SAED) confirms the crystalline nature of **Zn-(D-GluBenz)** as shown in Fig. 2d. The EDX and elemental mapping also confirmed the elemental composition and uniform distribution of **Zn-(D-GluBenz)** (Fig. 2g–i). The solid-state diffused reflectance spectrum (200–700 nm; KBr as reference medium) was also recorded to explore its optical properties (Fig. S8). On analysis, three peaks were observed, in which two peaks at 240 nm and 285 nm correspond to (π–π^*) transitions and one peak at 330 nm corresponds to (n–π^*) transition. These are all ligand-based transitions.

To check permanent porosity in **Zn-(D-GluBenz)**, the N_2 sorption was measured at 77 K. For this measurement, the fine powder of **Zn-(D-GluBenz)** was heated at 120 °C under vacuum to activate the sample. The maximum nitrogen

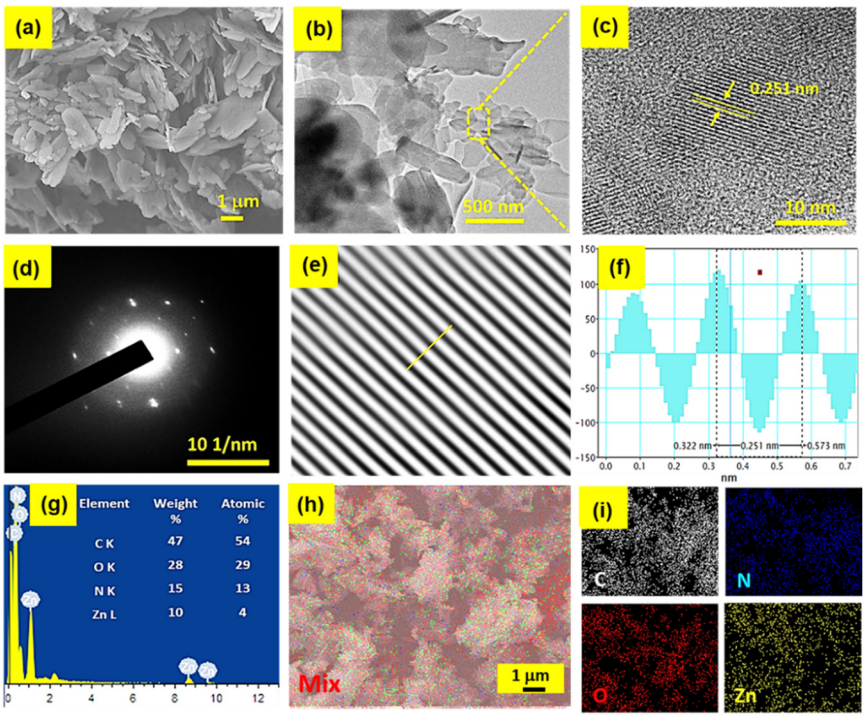

Fig. 2 (a) FESEM image, (b) TEM image, (c) HRTEM image, (d) selected area electron diffraction pattern, (e) lattice fringes, (f) average *d*-spacing, (g) energy dispersive X-ray (EDX) elemental spectrum with composition results, and (h and i) elemental mapping images of **Zn-(D-GluBenz)**.

uptake was found to be 38.1 cm^3 g^{-1}, which exhibits a type IV reversible isotherm (Fig. S9). A combination of H3 and H4 types of isotherms reveals the formation of wedge and slit-shaped pores between the agglomerated flakes.[38,39,41] The Brunauer–Emmett–Teller (BET) surface area is low, with a value of 13.5 m^2 g^{-1}, due to infrequent N_2 interaction sites. The non-linear DFT simulation was utilized to obtain the pore size distribution, which revealed a combination of mesoporous and microporous nature of the framework with two types of pore diameters, 1.28 and 3.7 nm (inset, Fig. S9).

To confirm the uncoordinated COOH site in **Zn-(D-GluBenz)**, an NH_3-TPD experiment was performed. The NH_3-TPD profile exhibits two distinct desorption peaks (Fig. S10). A high-temperature peak at 280 °C arises from the interaction of ammonia with the –COOH sites. In evaluating this peak, a quantitative value of the –COOH peak is found to be 0.655 mmol g^{-1}. Additionally, a low-temperature peak around 125 °C is also observed. This corresponds to the weakly bound ammonia associated with the Lewis acidic metal sites. In the latter case, the value (0.356 mmol g^{-1}) is more than half of the first peak.

Catalysis

In this catalysis, the synergistic role of both –NH and –COOH sites was demonstrated in the Friedel–Crafts alkylation reaction between indoles and β-nitrostyrenes shown at the top of Table 1.

Optimization of reaction conditions. To establish the best reaction conditions for the Friedel–Crafts alkylation reaction, the catalytic activity of **Zn-(D-GluBenz)** was assessed with variable solvents, times, temperatures and catalyst loadings. All conversion (%) results for catalysis reactions were obtained from ^{1}H NMR spectroscopy (Fig. S11–S15). For the initial standard analysis, a reaction between indole (0.15 mmol) and β-nitrostyrene (0.1 mmol) was performed using 4 mol% (5.6 mg) of catalyst at 27 °C for 12 h in CH_2Cl_2 solvent. The calculated conversion (%) was 39% (entry 1, Table 1). To comprehend the effect of solvent on the catalytic activity, other solvents like $CHCl_3$ (9%), MeOH (32%), EtOH (33%) and toluene (12%) were also screened as reaction media (entries 2–5, Table 1). On the other hand, the possibility of solvent-free reaction conditions was also explored, which barely promoted the catalysis with 7% conversion (entry 6, Table 1). Based on solvent analysis results, CH_2Cl_2 was used with an increase in temperature from 27 °C to 35 °C, considering the boiling point of CH_2Cl_2. A very minimal increase in conversion (%) from 39% to 41% (entry 7, Table1) suggested verifying other solvents under higher temperature conditions. Consequently, the reactions with solvents such as $CHCl_3$ (82%), EtOH (40%), and toluene (17%) were performed at 45 °C (entries 8–10, Table 1).

Table 1 Optimization of the reaction conditions[a]

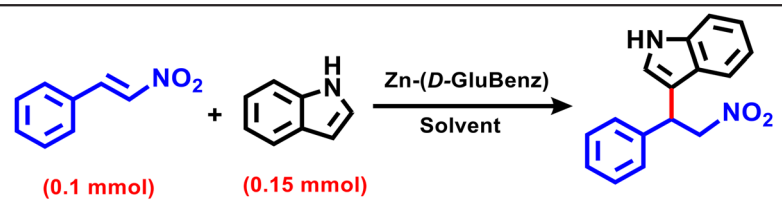

Entry	Catalyst (mol%)	Solvent	Temp. (°C)	Time (h)	Conversion[b] (%)
1	4	CH_2Cl_2	27	12	39
2	4	$CHCl_3$	27	12	09
3	4	MeOH	27	12	32
4	4	EtOH	27	12	33
5	4	Toluene	27	12	12
6	4	—	27	12	7
7	4	CH_2Cl_2	35	12	41
8	4	$CHCl_3$	45	12	82
9	4	EtOH	45	12	40
10	4	Toluene	45	12	17
11	4	CH_2Cl_2	35	18	43
12	4	CH_2Cl_2	35	24	45
13	4	$CHCl_3$	45	24	98
14	3	$CHCl_3$	45	24	98
15	2	$CHCl_3$	45	18	92
16	2	$CHCl_3$	45	24	97
17[c]	2	$CHCl_3$	45	24	0
18[c]	2	$CHCl_3$	45	24	23
19[d]	2	$CHCl_3$	45	24	98
20[e]	—	$CHCl_3$	45	24	0

[a] Reaction conditions: indole (0.15 mmol), β-nitrostyrene (0.1 mmol), solvent 1 mL and **Zn-(D-GluBenz)** as a catalyst for entries 1–16. [b] Determined by ^{1}H NMR spectroscopy. [c] Entries 17–18 were performed in the presence of $Zn(OAc)_2{\cdot}2H_2O$ and H_3(D-GluBenz), respectively. [d] Entry 19 was carried out with activated **Zn-(D-GluBenz)** catalyst. [e] Entry 20 was carried out without the use of any catalyst.

To optimize time as a reaction parameter, the increase in time from 12 h to 18 h (43%) (entry 11, Table 1) and 24 h (45%) (entry 12, Table 1) was executed in CH_2Cl_2 at 35 °C. This negligible increase in conversion (%) confirms that CH_2Cl_2 was not the choice of solvent for this reaction, even after giving the highest product conversion (%) at room temperature (27 °C). Following the result with $CHCl_3$ as a solvent at 45 °C in 12 h (entry 8, Table 1), the subsequent optimization of reaction conditions was carried out with $CHCl_3$ solvent.

Thus, using $CHCl_3$ as the solvent at 45 °C for 24 h with 4 mol% catalyst loading resulted in 98% product conversion (entry 13, Table 1). The observed result with catalyst loading 4 mol%, provided the scope to lower the catalyst amount from 4 mol% (5.6 mg) to 3 mol% (4.2 mg). Interestingly, the conversion (%) remained completely unaffected by this decrease in catalyst loading (entry 14, Table 1). On decreasing the catalyst load to 2 mol% (2.8 mg) and time to 18 h, 92% conversion was obtained (entry 15, Table 1). Thus, keeping the catalyst load at 2 mol%, an increase in time to 24 h provided 97% conversion (entry 16, Table 1). This detailed **Zn-(D-GluBenz)** catalytic activity analysis verified the finalized optimized reaction conditions with 2 mol% catalyst loading at 45 °C in 24 h with $CHCl_3$ as reaction medium (entry 16, Table 1). Fig. 3 demonstrates the time-dependent progress of this reaction under optimized reaction conditions. The ^{1}H NMR spectra showcase the increase of product formation on increasing the time from 1 h (0% conversion) to 24 h (97%).

Two control runs were conducted with $Zn(OAc)_2{\cdot}2H_2O$ and H_3(D-GluBenz) that were used in the synthesis of **Zn-(D-GluBenz)** as catalysts (entries 17–18, Table 1) under similar reaction conditions. $Zn(OAc)_2{\cdot}2H_2O$ gave no conversion, whereas H_3(D-GluBenz) gave 23% conversion. Furthermore, using activated **Zn-(D-GluBenz)** (at 120 °C under vacuum for 4 h) did not make any significant change in the product conversion (%) (entry 19, Table 1). In addition, a necessary control experiment without using a catalyst was also carried out (entry 20, Table 1). The results from these four control experiments confirmed the importance of the **Zn-(D-GluBenz)** for this catalysis, where the ligand functionalities are prime catalytic sites (the prevention of self-aggregation of ligands enhanced the overall catalytic activity), and the Zn(II) center does not play any role in the reaction.

Substrate scope. The productivity of a catalyst is always validated by its proficiency over a broad range of substrates, which is vital for pharmaceutical applications. To prove the efficacy of **Zn-(D-GluBenz)**, a wide variety of substrates for β-nitrostyrenes were examined. Under the optimized reaction conditions (2 mol% catalyst loading at 45 °C in $CHCl_3$ solvent in 24 h), all the substrates produced their respective alkylated products with good to excellent yields. To study the impact of electron-releasing groups (ERGs) and electron-withdrawing groups (EWGs) on the catalyst activity, the substrates listed below with mono and di-substituted β-nitrostyrenes were examined in comparison to unsubstituted β-nitrostyrene (97%) (Fig. 4). In this analysis, firstly, two examples of both

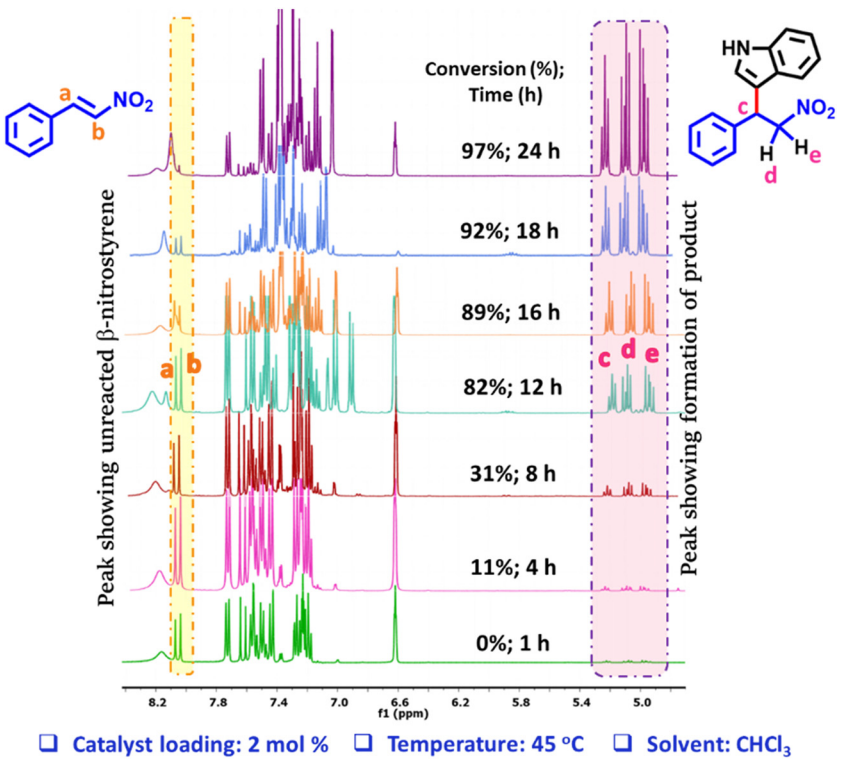

Fig. 3 ^{1}H NMR spectra in $CDCl_3$ showing time-dependent product formation.

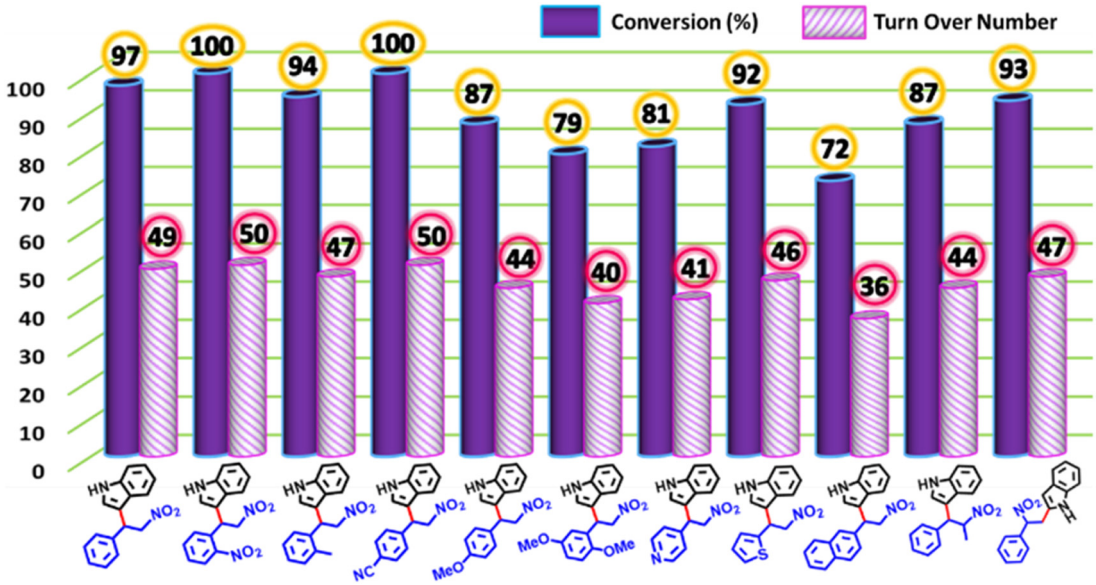

Fig. 4 Substrate scope with substituted β-nitrostyrenes showing conversion (%) and turnover numbers obtained under the chosen optimized reaction conditions using the **Zn-(D-GluBenz)** catalyst.

EWG and ERG cases with substitution at the *ortho* positions of the benzene ring were taken. 2,β-dinitrostyrene gave an excellent 100% product conversion, while 2-methyl-β-nitrostyrene gave a comparatively lesser (94%) product conversion. Further, two more examples with *para*-substitution on the benzene ring of the EWG and ERG were analyzed. In these examples o, 4-cyano-β-nitrostyrene (100%) gave better results than 4-methoxy-β-nitrostyrene (87%). Increasing the electron-releasing effect with the substitution at both *ortho* and *para* positions with 2,4-dimethoxy-β-nitrostyrene (79%) resulted in an even greater decrease in product conversion. All these results revealed that the EWG favors catalysis better than the ERG by increasing the electrophilic character of the aliphatic carbon atom for the attack on the indole moiety, which corroborates the mechanism of the reaction explained below. Two examples of heteroaromatic rings instead of benzene rings were also analyzed for more variety. Both (*E*)-4-(2-nitrovinyl) pyridine and (*E*)-2-(2-nitrovinyl)thiophene gave good product conversion at 81% and 92% due to their basic nature, respectively.

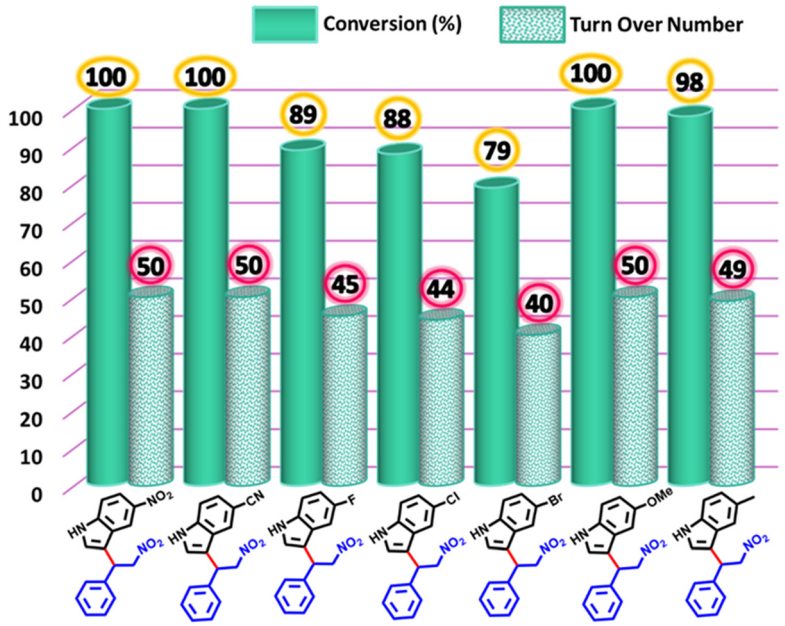

Fig. 5 Substrate scope with substituted indoles showing conversion (%) and turnover numbers obtained under the chosen optimized reaction conditions using the **Zn-(D-GluBenz)** catalyst.

Similarly, replacing the benzene ring with a naphthalene ring also decreased product conversion to 72% due to its electron-rich nature. On the other hand, substitution on the aliphatic chain, β-methyl-β-nitrostyrene, also gave a good 87% product conversion. Furthermore, instead of β-nitrostyrene, we used α-nitrostyrene with indole, giving an excellent 93% product conversion. To show the caliber of **Zn-(D-GluBenz)** catalyst, the substrate scope was further explored with substituted indoles (Fig. 5).

In this case also, both EWGs and ERGs were examined. For EWGs, 5-nitroindole and 5-cyanoindole were reacted with β-nitrostyrene. In both substrates, 100% conversion was obtained. In the case of halogen-substituted indoles, 5-fluoroindole, 5-chloroindole, and 5-bromoindole were utilized. As expected, with a decrease in the electronegativity from fluorine to bromine, the conversion percentage also decreased from 89% to 79%. Regarding ERGs, two standard examples of 5-methoxyindole and 5-methylindole were analyzed. In both cases, excellent product conversion was obtained with 100% and 98%, respectively. These results give an extreme understanding of variable substrates and the catalytic mechanism. All conversion (%) results for catalysis reactions were obtained from ^{1}H NMR spectroscopy, as shown in Fig. S16–S32. As an example, several products were isolated in pure form with 85% to 97% yields. The labelled ^{1}H and ^{13}C NMR spectra are shown in Fig. S33–S48. A comparison with other HBD catalysts reported in the literature confirmed the dignified place of **Zn-(D-GluBenz)** among the class of successful heterogeneous catalysts. In this comparative study, we also included some other metal-based MOFs with respect to catalyst loading, solvent, temperature, time, and product yield (Table S1). In the first example, a very high amount (43.5 mol%) of $[Zn_2(CO_2)_2(ATz)_4]$ (FCG-4) having a flanked $-NH_2$ functionality was used to achieve 97% conversion/yield at 60 °C in 10 h in toluene.[28] In the second example, 5 mol% of the urea moieties in an entangled framework $[Zn_2(azdc)_2(L)_2]\cdot 2DMF\cdot 2.5EtOH\cdot 3.5H_2O$ helped to achieve 100% yield at 60 °C in 16 h in acetonitrile solvent.[42] In another example, 5 mol% of a postsynthetically modified sulfate-based $[Zn_3(bpy)_3(SO_4)_4]\cdot(Me_2NH_2)_2\cdot DMF\cdot 9H_2O$ (transmetalated with Cu(II)) provided 98% yield in $CHCl_3$ in 16 h at 60 °C.[29] On the other hand, 22 mol% of a urea-based $[Zn_4O(L_2)(DMF)_2]\cdot 3DMF$ was required to get 90% yield in toluene at 60 °C in 24 h.[30] For further comparison, 5 mol% of the microporous ZIF-8 nanocrystals grown within the superhydrophobic porous polymer (PDVB-vim) in the composite of ZIF-8/PDVB vim provided 99% yield in acetonitrile at 25 °C in 24 h.[43] In the next example, the 2D Ln-MOF $[La_{2/3}(qptca)_{1/2}]$ was utilized as a catalyst to get a 93% yield with 1.8 mol% catalyst loading at 80 °C in 12 h in ^{n}PrOH solvent.[31] For the Co(II) based CSMCRI-21a framework, 3.6 mol% loading was required for 97% yield in toluene at 60 °C in 12 h.[36] Interestingly, 3 mol% of the primary amide containing $\{[Zn_2(2\text{-BQBG})(BDC)_2]\cdot 10H_2O\}_n$ was utilized to get 100% yield in toluene solvent at 12 h at 35 °C.[35] For the last example, urea-tethered porous organic polymer (IPpop-1) was utilized using EtOH as solvent at 50 °C for 12 h with a high catalyst loading (10 mg).[32] All of the catalysts reported in the literature required either very high catalyst loading and/or comparatively higher reaction temperatures. Along with all complex synthesis processes, their catalytic conditions and non-availability of a clear arrangement of the HBD sites in these examples still result in a similar product yield. Therefore, the easy synthesis process requiring cheap starting materials under milder reaction conditions confirms the merits of **Zn-(D-GluBenz)** for the Friedel–Crafts alkylation reaction.

Heterogeneity and leaching test. The impactful catalysts are those that overcome the drawbacks of traditional catalysts. Homogeneity is one such drawback in the case of traditional organic catalysts, while the use of metal-based catalysts has leaching issues into valuable products. These two drawbacks are major concerns in the catalysis industry. Therefore, in this study, we have shown excellent heterogeneity and non-leaching characteristics of the **Zn-(D-GluBenz)** catalyst. For the heterogeneity test, the catalyst was removed by centrifugation from the typical reaction after 4 h, and the reaction was resumed to observe the progress of the reaction. The observed results showed that the reaction progressed very slowly with 11%, 16%, 21%, 23%, 24% and 26% conversion in 4 h, 8 h, 12 h, 16 h, 18 h and 24 h, respectively (Fig. 6, purple line). On the other hand, the reaction was completed in the presence of **Zn-(D-GluBenz)** (Fig. 6, pink line). This primarily confirmed the heterogeneous nature of **Zn-(D-GluBenz)** and its importance in the reaction. Further, the crude product obtained after 24 h of reaction was analyzed for Zn(II) metal ions. The crude organic part was extracted from the reaction by evaporating the solvent under vacuum and dried overnight. The sample was analyzed using energy-dispersive X-ray (EDX) spectroscopy, in which the

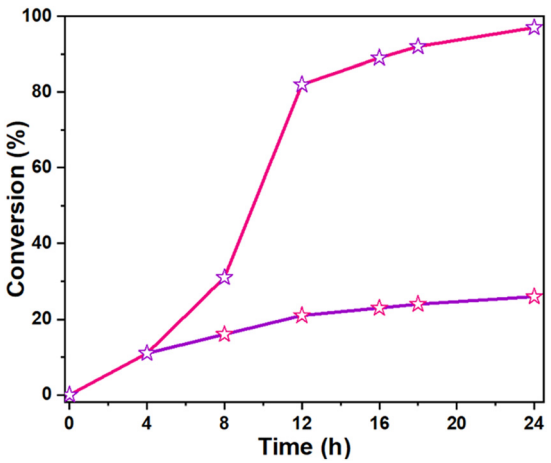

Fig. 6 Plot of conversion (%) *versus* time for the **Zn-(D-GluBenz)** catalyst. The purple line represents the reaction progress after catalyst removal at 4 h, while the pink line shows product conversion over 24 h with the catalyst present.

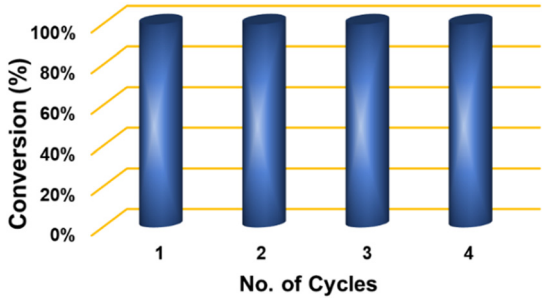

Fig. 7 Product conversion for four successive catalytic cycles.

elemental mapping confirmed the absence of any trace amount of Zn (Fig. S49). This verified that **Zn-(D-GluBenz)** did not leach into the reaction mixture during catalysis.

Recyclability and stability test. The convincing capability of a catalyst is always judged by its recyclability and stability for multi-catalytic cycles. Analyzing the recycling capability of **Zn-(D-GluBenz)** up to four successive runs with indole and β-nitrostyrene validated its potency as a catalyst. As expected, there is no evident loss in conversion percentage even after four cycles, as shown in Fig. 7.

To depict the stability of the catalyst, it was separated after four successive catalytic runs for FTIR, PXRD and FESEM analysis. Expectedly, it was found that the structural integrity of **Zn-(D-GluBenz)** was intact after all the catalytic cycles (Fig. S50–S52). Therefore, these post-catalytic experimental data confirmed the catalyst quality among many heterogeneous catalysts in the literature reports.

Mechanistic aspect. For the credible mechanism of the Friedel–Crafts alkylation, the literature studies involving indole and β-nitrostyrene as reactants were considered.[35,36] There is no role of unsaturated metal as Lewis acidic sites in the mechanism of the reaction, which was also confirmed by using both unactivated and activated **Zn-(D-GluBenz)** catalysts (entries 16 and 19, Table 1). In this catalyst, the prime catalytic sites are HBD sites present in the ligand as uncoordinated –COOH and –NH groups. Only the ligand part is shown in Fig. 8a to clarify the interaction with these catalytic sites in the catalytic mechanism. At the onset of step 1, both –COOH and –NH groups, due to their close proximal arrangement, simultaneously form hydrogen bonding with the $-NO_2$ group of β-nitrostyrene. This hydrogen bonding interaction activates the β-nitrostyrene for nucleophilic attack in step 2 by the indole due to an increase in electrophilicity of the α-carbon atom. Concomitantly, the interaction of the –NH group of the indole with the oxygen atom of the –COOH group increases the nucleophilic nature of the indole moiety. These simultaneous interactions of both reactants bring them in the vicinity of each other to instigate the formation of an alkylated product through the delocalization of electron density and finally avail the catalyst in step 4 for the next catalytic cycle. To validate the interaction of the catalyst with β-nitrostyrene, the fluorometric titrations were performed based on the luminescence property of **Zn-(D-GluBenz)**. For this sensing experiment, the homogeneous dispersion of 2 mg of finely powdered **Zn-(D-GluBenz)** was prepared in 2 mL $CHCl_3$. Using this dispersion, the emission spectra were recorded at an excitation wavelength of 280 nm with an incremental addition of a freshly prepared 2 mM solution of β-nitrostyrene in $CHCl_3$. A sharp decrease in the intensity was observed on the consecutive addition of every 10 mL of β-nitrostyrene solution (Fig. 8b). On addition of a total of 50 μL β-nitrostyrene, the observed 74% quenching confirms the

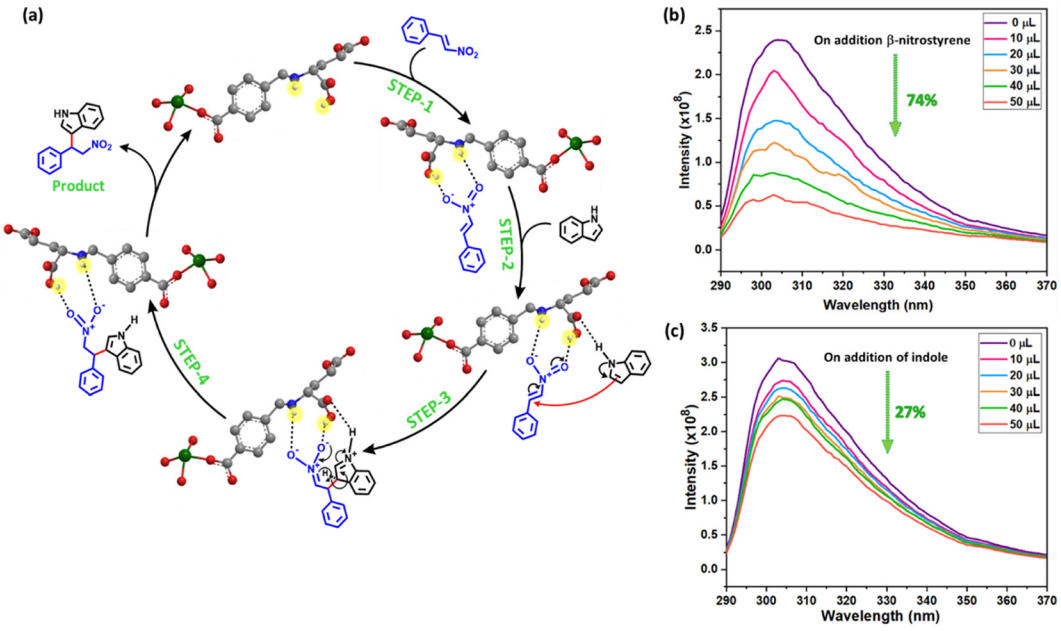

Fig. 8 (a) Propounded catalytic cycle and (b and c) emission spectra (λ_{ex} = 280 nm) of homogeneous dispersion of **Zn-(D-GluBenz)** in chloroform on incremental addition of 2 mM solution of β-nitrostyrene and indole, respectively.

strong hydrogen bonding interaction. In a similar experiment with the addition of a 50 μL 2 mM solution of indole to the dispersed catalyst, a comparatively lower (27%) change in intensity is observed (Fig. 8c). For their cumulative effect, another experiment with 50 μL of β-nitrostyrene followed by 50 μL of indole showed an overall 83% quenching (Fig. S53). This shows that β-nitrostyrene actually has a stronger hydrogen bonding interaction with **Zn-(D-GluBenz)** than indole.

Conclusions

In summary, we exemplified the synthesis of **H_3(D-GluBenz)** ligand and its utilization for making a new 3D MOF, namely $[Zn_4(H(D\text{-}GluBenz))_4(H_2O)_2]_n$ denoted as **Zn-(D-GluBenz)**. In addition to its thermal robustness, the **Zn-(D-GluBenz)** MOF exhibited noteworthy structural stability. The FTIR characterization also revealed the presence of pendant –COOH functionalities within the framework. The strategically decorated **Zn-(D-GluBenz)** with an uncoordinated –COOH and –NH moiety oriented in the vicinity of each other as the HBD sites was utilized for the Friedel–Crafts alkylation of indoles and β-nitrostyrenes. With the synergistically accessible HBD sites, we were able to showcase better reaction conditions for this reaction compared to higher catalyst loading and elevated reaction temperature in the literature reports. Control studies with activated **Zn-(D-GluBenz)** confirmed that the catalytic activity arose solely from HBD sites, with Lewis acidic sites showing no involvement. We have also demonstrated the extensive range of substrates in eminent yields under optimized reaction conditions. The recyclability and heterogeneity test displayed the catalyst's quality. The **Zn-(D-GluBenz)** catalyst was highly stable after four consecutive catalytic runs, as confirmed by FESEM and PXRD analysis. Strong experimental support for the proposed catalytic mechanism was provided by fluorescence studies, which revealed a significant reduction in the emission intensity of **Zn-(D-GluBenz)** upon incremental addition of β-nitrostyrene. This pronounced quenching effect highlights the hydrogen bonding interaction between both –COOH and –NH groups of the catalyst and the nitro group of β-nitrostyrene, thereby affirming the crucial role of these interactions in substrate activation. Based on this work, we plan to extend the importance of the synergistic effect of HBD sites by the ornamentation of –COOH and –NH in the framework for other organic transformations.

Data availability

Data for this work is presented in this manuscript along with the supplementary information (SI) file.

Supplementary information: materials and physical methods, FTIR, NMR, HRMS, CD spectra, PXRD, DRS, structure optimization by Materials Studio, BET surface area, pore size, FESEM, EDX and emission spectra. See DOI: **https://doi.org/10.1039/d5cy00966a**.

Conflicts of interest

There are no conflicts to declare.

Acknowledgements

This research was supported by IISER Mohali. V. S. acknowledges the Ministry of Education, India, for providing a research fellowship. The authors also thank IISER Mohali for access to central facilities (NMR, HRMS, X-ray, FESEM, and TEM) as well as the CHN facility at IIT Bombay.

References

1 A. G. Doyle and E. N. Jacobsen, *Chem. Rev.*, 2007, **107**, 5713–5743.
2 J. Werth and M. S. Sigman, *J. Am. Chem. Soc.*, 2020, **142**, 16382–16391.
3 T. J. Auvil, A. G. Schafer and A. E. Mattson, *Eur. J. Org. Chem.*, 2014, 2633–2646.
4 P. R. Schreiner, *Chem. Soc. Rev.*, 2003, **32**, 289–296.
5 M. J. Gaunt, C. C. C. Johansson, A. McNally and N. T. Vo, *Drug Discovery Today*, 2007, **12**, 8–27.
6 A. Das, N. Anbu, M. Sk, A. Dhakshinamoorthy and S. Biswas, *Inorg. Chem.*, 2019, **58**, 5163–5172.
7 H. Furukawa, K. E. Cordova, M. O'Keeffe and O. M. Yaghi, *Science*, 2013, **341**, 1230444.
8 A. Dhakshinamoorthy and H. García, *Chem. Soc. Rev.*, 2014, **43**, 5750–5765.
9 B. Liu, M. Jiang, D. Zhu, J. Zhang and G. Wei, *Chem. Eng. J.*, 2022, **428**, 131118.
10 V. Subramaniyam, P. V. Ravi and M. Pichumani, *J. Mol. Struct.*, 2022, **1251**, 131931.
11 C. Zhu, H. Tang, K. Yang, X. Wu, Y. Luo, J. Wang and Y. Li, *Catal. Commun.*, 2020, **135**, 105837.
12 A. Das, N. Anbu, M. Sk, A. Dhakshinamoorthy and S. Biswas, *ChemCatChem*, 2020, **12**, 1789–1798.
13 P. C. Rao and S. Mandal, *Chem. – Asian J.*, 2019, **14**, 4087–4102.
14 A. Das and A. K. Das, *New J. Chem.*, 2023, **47**, 5347–5355.
15 A. S. Lawrence, B. Sivakumar, S. L. Rokhum, S. Biswas, F. G. Cirujano and A. Dhakshinamoorthy, *ChemCatChem*, 2024, **16**, e202401477.
16 R. B. Longmore and B. Robinson, *J. Pharm. Pharmacol.*, 1969, **21**, 118S–125S.
17 M. W. Majchrzak, J. N. Zobel and D. J. Obradovich, *Synth. Commun.*, 1997, **27**, 3201–3211.
18 S. Lancianesi, A. Palmieri and M. Petrini, *Chem. Rev.*, 2014, **114**, 7108–7149.
19 R. J. Sundberg, *The Chemistry of Indoles*, Academic Press, New York, 1996.
20 J. A. Joule, *Med. Chem. Commun.*, 2010, **1**, 15–28.
21 M. Bandini and A. Eichholzer, *Angew. Chem., Int. Ed.*, 2009, **48**, 9608–9644.
22 M. Rueping and B. J. Nachtsheim, *Beilstein J. Org. Chem.*, 2010, **6**, 6.

23 O. M. Berner, L. Tedeschi and D. Enders, *Eur. J. Org. Chem.*, 2002, 1877–1894.
24 G. Dessole, R. P. Herrera and A. Ricci, *Synlett*, 2004, **13**, 2374–2378.
25 E. A. Hall, L. R. Redfern, M. H. Wang and K. A. Scheidt, *ACS Catal.*, 2016, **6**, 3248–3252.
26 A. H. Chughtai, N. Ahmad, H. A. Younus, A. Laypkov and F. Verpoort, *Chem. Soc. Rev.*, 2015, **44**, 6804–6849.
27 F. Ghobakhloo, M. Mohammadi, M. Ghaemi and D. Azarifar, *ACS Appl. Nano Mater.*, 2024, **7**, 1265–1277.
28 R. Chand, A. S. Palakkal, M. Neem and S. Neogi, *Small*, 2025, **21**, 2501767.
29 W. P. Zhong, Q. W. Chen, X. X. Cao, S. L. Liu, Q. Chen and N. Lin, *Inorg. Chem. Commun.*, 2020, **119**, 108037.
30 P. C. Rao and S. K. Mandal, *ChemCatChem*, 2017, **9**, 1172–1176.
31 J. Q. Wu, X. Y. Wu, J. M. Lu, Q. Shi and L. X. Shao, *Chem. – Eur. J.*, 2022, **28**, e202200174.
32 G. K. Dam, S. Let, V. Jaiswal and S. K. Ghosh, *ACS Sustainable Chem. Eng.*, 2024, **12**, 3000–3011.
33 J. M. Roberts, B. M. Fini, A. A. Sarjeant, O. K. Farha, J. T. Hupp and K. A. Scheidt, *J. Am. Chem. Soc.*, 2012, **134**, 3334–3337.
34 C. M. McGuirk, M. J. Katz, C. L. Stern, A. A. Sarjeant, J. T. Hupp, O. K. Farha and C. A. Mirkin, *J. Am. Chem. Soc.*, 2015, **137**, 919–925.
35 D. Markad and S. K. Mandal, *ACS Catal.*, 2019, **9**, 3165–3173.
36 N. Seal and S. Neogi, *Chem. Commun.*, 2023, **59**, 4954–4957.
37 M. Agirre, A. Arrieta, I. Arrastia and F. P. Cossío, *Chem. – Asian J.*, 2019, **14**, 44–66.
38 V. Sharma and S. K. Mandal, *ACS Appl. Nano Mater.*, 2023, **6**, 20028–20037.
39 V. Gupta and S. K. Mandal, *Chem. – Eur. J.*, 2020, **26**, 2658–2665.
40 Dassault Systèmes and BIOVIA, *ViewerLite 5.0*, Dassault Systèmes, San Diego, 2002.
41 D. Khan, L. Qiu, C. Liang, K. Mirza, M. Kashif, B. Yang, K. L. Kra, Y. Wang and X. Li, *ACS Omega*, 2022, **7**, 10820–10839.
42 M. Singh and S. Neogi, *Inorg. Chem.*, 2023, **62**, 871–884.
43 M. L. Gao, S. Liu, L. Liu and Z. B. Han, *Nanoscale*, 2024, **16**, 10637–10644.